

Modeling of particle agglomeration in nanofluids

K. Hari Krishna, S. Neti, A. Oztekin, and S. Mohapatra

Citation: *Journal of Applied Physics* **117**, 094304 (2015); doi: 10.1063/1.4913874

View online: <http://dx.doi.org/10.1063/1.4913874>

View Table of Contents: <http://scitation.aip.org/content/aip/journal/jap/117/9?ver=pdfcov>

Published by the [AIP Publishing](#)

Articles you may be interested in

[A thermal conductivity model of nanofluids based on particle size distribution analysis](#)

Appl. Phys. Lett. **105**, 083117 (2014); 10.1063/1.4894254

[Role of surface charge, morphology, and adsorbed moieties on thermal conductivity enhancement of nanofluids](#)

Appl. Phys. Lett. **101**, 173113 (2012); 10.1063/1.4764050

[Effects of p H on heat transfer nanofluids containing ZrO₂ and TiO₂ nanoparticles](#)

J. Appl. Phys. **109**, 024305 (2011); 10.1063/1.3532003

[The limiting behavior of the thermal conductivity of nanoparticles and nanofluids](#)

J. Appl. Phys. **107**, 114319 (2010); 10.1063/1.3354094



[Comment on "Particle concentration and tube size dependence of viscosities of Al₂O₃—water nanofluids flowing through micro- and minitubes" \[*Appl. Phys. Lett.*91, 243112 \(2007\)\]](#)

Appl. Phys. Lett. **94**, 066101 (2009); 10.1063/1.3078393



AIP | Journal of Applied Physics

Meet The New Deputy Editors

	Christian Brosseau		Laurie McNeil		Simon Phillpot
---	---------------------------	---	----------------------	---	-----------------------

Modeling of particle agglomeration in nanofluids

K. Hari Krishna,¹ S. Neti,¹ A. Oztekin,¹ and S. Mohapatra²

¹*Department of Mechanical Engineering and Mechanics, Lehigh University, 19W Memorial Dr, Bethlehem, Pennsylvania 18015, USA*

²*Dynalene Inc., 5250W Coplay Rd, Whitehall, Pennsylvania 18052, USA*

(Received 21 October 2014; accepted 14 February 2015; published online 5 March 2015)

Agglomeration strongly influences the stability or shelf life of nanofluid. The present computational and experimental study investigates the rate of agglomeration quantitatively. Agglomeration in nanofluids is attributed to the net effect of various inter-particle interaction forces. For the nanofluid considered here, a net inter-particle force depends on the particle size, volume fraction, pH, and electrolyte concentration. A solution of the discretized and coupled population balance equations can yield particle sizes as a function of time. Nanofluid prepared here consists of alumina nanoparticles with the average particle size of 150 nm dispersed in de-ionized water. As the pH of the colloid was moved towards the isoelectric point of alumina nanofluids, the rate of increase of average particle size increased with time due to lower net positive charge on particles. The rate at which the average particle size is increased is predicted and measured for different electrolyte concentration and volume fraction. The higher rate of agglomeration is attributed to the decrease in the electrostatic double layer repulsion forces. The rate of agglomeration decreases due to increase in the size of nanoparticle clusters thus approaching zero rate of agglomeration when all the clusters are nearly uniform in size. Predicted rates of agglomeration agree adequate enough with the measured values; validating the mathematical model and numerical approach is employed. © 2015 AIP Publishing LLC.

[<http://dx.doi.org/10.1063/1.4913874>]

I. INTRODUCTION

Colloid science has seen substantial progress since its early days in the 1860s. Many factors go into establishing a stable colloidal dispersion, as solid colloids tend to agglomerate at favorable conditions and can settle when particle density is larger than that of the medium. One application of solid colloids is in thermal fluids, since it has been reported that dispersions of solid nanoparticles in heat transfer fluids could enhance their thermal properties. Clogging and settling have been reported in colloids containing micron size particles. This has in turn created some interest into the understanding colloidal dispersions with nano-particles.

Owing to their small size and relatively large surface area, nanoparticles dispersed in the nanofluids have created considerable interest in recent times for their improved heat transfer and other properties. Generally, a distribution of sizes results when nanoparticles are manufactured, and the average particle size and standard deviation are used to define the particles. Park *et al.*¹ observed that standard deviation of the particle size distribution (PSD) can be controlled by controlling the aggregation of particles during production. Pioneering researchers at Argonne National Laboratory [Eastman *et al.*,² Lee *et al.*³] started experimenting with nanofluids to analyze the heat transfer characteristics. Unfortunately, many nanofluids have been found to be unstable with settling being visually observed. Such behavior was attributed to the coagulation or agglomeration and sedimentation of the agglomerates. The present work hopes to shed some light on the causes for such instability.

Agglomeration is a process in which colloidal particles mutually interact as part of Brownian motion, and combine

with adjacent ones to form clusters of particles. During the agglomeration, particles in clusters experience a net attractive force which depending on the conditions requires greater than the amount of local energy necessary to bring them apart. This attractive force is known as Van der Waals force, which at molecular level is due to the interaction between dipoles on molecules. According to London theory [London⁴], the interaction energy $V_{int}(R)$ (Eq. (1)) is inversely proportional to the sixth power of the separation (R) between molecules.

$$V_{int}(R) \propto \frac{1}{R^6}. \quad (1)$$

Summation of all the intermolecular forces between the colloidal particles is close to the long-range Van der Waals interaction (negative force) of the colloid. If there are no other interparticle forces, then the particles cling together due to the attractions resulting in cluster formations. As the particle size increases, the larger particles could settle down. Agglomeration could be controlled or altered by changing surface properties of the colloidal particles by introducing surface charges, and/or by forming polymer layers around the particles that generate repulsive forces between the particles and thus keep them apart from forming clusters. Interparticle agglomeration is studied in the current work.

Forces and factors affecting agglomeration, and the effects of agglomeration on rheological and heat transfer characteristics of nanofluids are analyzed here. Islam *et al.*⁵ have reviewed the modified expressions for interaction energies and stability ratios in colloids by including the hetero-aggregation effects that affect the interaction between the particles with different sizes, shapes, surface charge, etc., in

dispersion medium. Das *et al.*⁶ investigated heat transfer characteristics of non-functionalized alumina nano-particles at different concentrations at low pH values without stabilizers/surfactants. Their sonicated fluid remained stable for about 6 h, and then the particles settled. With increase in concentration, the settling increased implying increase in the agglomeration with concentration. Lo and Tsung⁷ observed that agglomeration in CuO nanofluid increased with increase in time, but no consistent trend in the increase of average particle size was observed with independent variables such as temperature. Lee *et al.*⁸ studied the influence of the surface charge on particle aggregation in nanofluids by regulating the particle surface charge with pH. They observed increase in the surface charge with decrease in pH from the isoelectric point, which could be due to increase in the concentration of potential-determining ions (H^+). With increase in the surface charge, they observed increase in the stability of the nanofluid which was attributed to the increase in the electrostatic repulsion energy between the nanoparticles. Thermal conductivity of the nanofluid increased with change in the pH away from the isoelectric point, and with increase in the volume fraction. Timofeeva *et al.*⁹ observed that 11 nm particles formed larger agglomerates than the 40 nm particles, and the size of the agglomerated particles increased with time. They also observed that the thermal conductivity of the alumina nanofluid increased slightly over time due to particle agglomeration. Lee *et al.*¹⁰ have prepared alumina nanofluids without surfactants with ultrasonication up to 20 h, and observed zeta potential to increase with the duration of ultrasonication, before reaching an asymptote. Yang *et al.*¹¹ reported increased agglomeration with time as evidenced by the increase in average particle size of the nanofluids. It was also observed that agglomeration in nanofluids has negligible effect on the thermal conductivity, although both thermal conductivity and viscosity increased with the volume fraction of nanofluids.

Based on the above described work, it appears that the size of nanoparticles in nanofluids increases with time due to agglomeration, which has a strong effect on viscosity and negligible effect on thermal conductivity of nanofluids. Due to agglomeration, large clusters of nanoparticles get sediment over time, thus losing its stability and properties as a nanofluid. It is evident that more than rheology and heat transfer characteristics, the stability or shelf-life of nanofluid could decide the usefulness of the nanofluid. The attractive or repulsive forces between two similar or dissimilar particles in a dispersion medium are attributable to the surface properties of particles. To better understand and control the agglomeration in nanofluids (with billions of nanoparticles), the combined effects of the surface interactions of particles and the effect of particle size distribution with time need to be analyzed.

The present work is aimed at quantitatively addressing the effect of agglomeration phenomenon in nanofluids with time, taking into consideration the interactions between nanoparticles of different sizes along with the effects of dispersion medium. A numerical model of the fluid has been developed that requires the solution of coupled population balance equations and obtain the particle size distributions at

different times. The independent variables of interest include volume fraction, particle size, pH, and electrolyte concentration and related ion concentrations and zeta potentials. The numerical model describing the nanofluid has been validated by comparing the results with experiments with alumina nanofluids.

II. MATHEMATICAL AND NUMERICAL METHOD

Population balance equations have diverse applications in many areas involving particulate systems like crystallization, aerosol dynamics, colloidal aggregation, etc. The balances are described using integro-partial differential equations with a general form for pure aggregation is given by

$$\frac{\partial n(v, t)}{\partial t} = \frac{1}{2} \int_0^v \beta(v-v', v') n(v-v', t) n(v', t) dv' - n(v, t) \int_0^\infty \beta(v, v') n(v', t) dv'. \quad (2)$$

Here, $n(v, t)$ is the number density of particles per unit volume of the nanofluid. The first term on right hand side of Eq. (2) corresponds to the "birth rate" of particulate clusters of volume/size v due to collisions of smaller particles with sizes $v-v'$ and v' , and the second term corresponds to the "death rate" of particles due to collisions with other particles to form particulate clusters of size $v + v'$. Other phenomena like nucleation and growth of particles can be included into the population balance equations by adding corresponding terms into Eq. (2). The kinetics of the agglomeration is attributed to the rate kernels $\beta(v-v', v')$ and $\beta(v, v')$ in the birth and death rate terms, respectively.

To solve the coupled population balance equations, the method of discretization is utilized. Kumar and Ramkrishna¹² have proposed a method of discretization in which the particles are distributed into different interval depending on the volume/size.

A particle size grid (Figure 1) for nanoparticles is considered with M intervals that can include all the sizes of particles in the nanofluids. v_1 and v_{M+1} correspond to the size of smallest and largest particles in nanofluid. Representative size (x_i) has been assigned to all the particles in a particular interval and related to the end volume of each interval as $v_i = (x_i + x_{i+1})/2$. The grid can be uniform or geometric type ($x_{i+1} = rx_i$) with varying coarseness. At a given time, t , the total number of particles in an interval is represented by $N_i(t)$, which is obtained from the number density distribution

$$N_i(t) = \int_{v_i}^{v_{i+1}} n(v, t) dv. \quad (3)$$

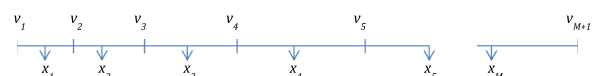


FIG. 1. Particle size grid with M intervals.

The non-dimensionalized and discretized population balance equation for the number of particles in i th interval can be shown to be an ordinary differential equation.

$$\frac{dN_i^*(t)}{dt^*} = (N_o t_o) \left\{ \sum_{v^* i \leq x^* j + x^* k \leq v^* i+1} \sum_{j \geq k} \left(1 - \frac{\delta_{jk}}{2}\right) \beta_{jk} N_j^*(t) N_k^*(t) - N_i^*(t) \sum_{k=1}^M \beta_{ik} N_k^*(t) \right\}. \quad (4)$$

N^* , x^* , v^* , t^* are the non-dimensionalized number of particles (N^*), representative volume (x^*), particle volume (v^*), and time constant (t^*), respectively. The number of particles in each interval is non-dimensionalized by the initial number of particles N_o per unit volume of dispersed medium, and the size of particles is non-dimensionalized by the initial average size/volume of particles V_o per unit volume of dispersed medium. This implies $N_o V_o$ would give the volume fraction of the nanofluid. Here, δ_{ij} is the Kronecker delta ("1" if $j=k$ and "0" if $j \neq k$) to ensure particles from a size interval are counted only once. To conserve the volume of nanoparticles in the nanofluid, Kumar and Ramkrishna¹² have proposed the use of Eq. (5).

$$\frac{dx_i^*(t)}{dt^*} = (N_o t_o) \frac{1}{N_i^*(t)} \sum_{v^* i \leq x^* j + x^* k \leq v^* i+1} \sum_{j \geq k} \left(1 - \frac{\delta_{jk}}{2}\right) \beta_{jk} (x_j^* + x_k^* - x_i^*) N_j^*(t) N_k^*(t). \quad (5)$$

In a particular interval of the grid (shown in Figure 1), if the number density of particles is more towards an end of the interval, then Eq. (5) adjusts the representative size of each interval such that the total volume of nanoparticles is preserved.

The numerical model takes the initial particle size distribution, solves the M coupled system of equations at each time interval, and marches forward in time to get the particle size distribution at different times. To get more accurate distributions, the size of the grid M and geometric width of the intervals are varied iteratively. In this study, grid size of 80 and geometric width of 1.15 are selected. In Eqs. (2), (4), and (5), the rate kernel β has different forms depending on the type of physical applications such as droplet coalescence, dispersions, polymers, granulation, etc., as consolidated by Rao.¹³

Smoluchowski¹⁴ has derived an expression for the collision frequency of particles in a dispersion medium based on Brownian motion, and obtained the Brownian collision rate β_b of two particles with sizes/volumes u , v and radii a_1 , a_2 as

$$\beta_b = 4\pi(D_1 + D_2)(a_1 + a_2) = \frac{2k_B T}{3\eta} \left(u^{-\frac{1}{3}} + v^{-\frac{1}{3}}\right) \left(u^{\frac{1}{3}} + v^{\frac{1}{3}}\right). \quad (6)$$

The diffusion coefficients of particles $D_1 = \frac{k_B T}{6\pi\eta a_1}$ and $D_2 = \frac{k_B T}{6\pi\eta a_2}$ are obtained from the Stokes-Einstein equation.

Here, k_B is the Boltzmann constant, T is the absolute temperature of particle medium, and η is the viscosity of particle medium. Not all interactions between particles dispersed lead to a permanent cluster formation. The stability ratio or the collision efficiency, W , given by Hunter and White¹⁵ is the ratio of the number of collisions between particles of radii a_1 , a_2 to the number of collisions that could result in coagulation between them.

$$W = 2 \int_2^\infty H_d \frac{\exp\left(\frac{V_T}{k_B T}\right)}{s^2} ds, \quad (7a)$$

$$s = \frac{2R}{a_1 + a_2}. \quad (7b)$$

V_T is the total interaction energy and H_d is the expression to incorporate the hydrodynamic drag forces between particles of radii a_1 and a_2 . According to the DLVO theory named after Deryaguin, Landau, Verwey, and Overbeek [Derjaguin and Landau,¹⁶ and Verwey and Overbeek¹⁷], two particles aggregate after interaction when the net energy in bringing the two particles to collide is attractive (negative). Total interaction energy V_T is the result of repulsive energy V_R due to electrostatic double layer repulsive forces, and attractive energy V_A due to Van der Waals attractive forces between the particles.

$$V_A = -\frac{A_H}{6} \left\{ \frac{2a_1 a_2}{R^2 - (a_1 + a_2)^2} + \frac{2a_1 a_2}{R^2 - (a_1 - a_2)^2} + \ln \left(\frac{R^2 - (a_1 + a_2)^2}{R^2 - (a_1 - a_2)^2} \right) \right\}. \quad (8)$$

Here, A_H is the effective Hamaker constant [Hamaker¹⁸] between two particles in the medium, and is observed to be positive for two particles of same material type. Between two alumina particles, the Hamaker constant A_H is 5.7×10^{-20} J. Electrostatic double layer repulsion energy between the particles, V_R is

$$V_R = \epsilon_o \epsilon_r \left(\frac{a_1 a_2}{R}\right) [(\psi_1 + \psi_2)^2 \ln(1 + e^{-\kappa H}) + (\psi_1 - \psi_2)^2 \ln(1 - e^{-\kappa H})]. \quad (9)$$

Here, ψ_1 and ψ_2 are the potentials on charged nanoparticles and are dependent on the surface charge density of the particles. R is the center-to-center distance between the interacting particles. Using Debye-Hückle theory of electrolytes [Debye and Huckle¹⁹], the thickness of the electrostatic double layer is expressed as $\kappa^{-1} = \sqrt{\frac{\epsilon_o \epsilon_r k_B T}{2N_A e^2 I}}$ in m . Here, ϵ_o is the permittivity of free space, ϵ_r is the relative permittivity of medium, N_A is the Avogadro number, e is the elementary charge, and I is sum of the concentration of all ions including the electrolyte ions other than the potential determining ions in the nanofluid. According to the theory, with increase in the electrolyte concentration I (mol m^{-3}), the Debye length decreases which in turn decreases stability of the nanofluid.

Equation (9) [Sader *et al.*²⁰] is applicable for all κH , and is a modified version of Hogg, Healy, and Fuerstenau (HHF) expression [Hogg *et al.*²¹]. As per Debye-Hückle approximation theory [Debye and Huckle¹⁹], expressions for all the potential energies are accurate for $\kappa \cdot a \gg 1$, where a is the radius of nanoparticle. For smaller potentials, zeta potential values can be used as the surface potential of the particles. H_d in Eq. (7a) is the correction factor to include the hydrodynamic drag effect on the particles in the medium, and can be given as,

$$H_d = \frac{6(s-2)^2 + 13(s-2) + 2}{6(s-2)^2 + 4(s-2)}, \quad (10a)$$

$$s = \frac{2R}{a_1 + a_2}. \quad (10b)$$

Using Eqs. (6)–(10a), the rate kernel for agglomeration β in a dispersion medium is written as

$$\begin{aligned} \beta &= \frac{1}{W} \beta_b \\ &= \frac{1}{2 \int_2^\infty H_d \frac{\exp\left(\frac{V_T}{k_B T}\right)}{s^2} ds} \left[\frac{2k_B T}{3\eta} (u^{-\frac{1}{3}} + v^{-\frac{1}{3}}) (u^{\frac{1}{3}} + v^{\frac{1}{3}}) \right]. \end{aligned} \quad (11)$$

By substituting this kernel β in the discretized population balance Eqs. (4) and (5), the particle size distribution at different times can be solved by the numerical model for a given initial particle size distribution of the nanofluid.

To validate the above numerical model, a constant rate kernel is used to solve the M coupled population balance equations. The obtained particle size distributions at different times are compared with the analytical solution for the particle number density at different times derived by Scott²² for a constant rate kernel.

$$n(v, 0) = \left(\frac{N_o}{V_o}\right) \left(\frac{4v}{V_o}\right) e^{-\left(\frac{2v}{V_o}\right)}, \quad (12)$$

$$n(v, t) = \left(\frac{N_o}{V_o}\right) \frac{8e^{-\left(\frac{2v}{V_o}\right)} \sinh \left\{ 2 \left(\frac{v}{V_o}\right) \left(\frac{T}{(T+2)^2}\right) \right\}}{T^{\frac{1}{2}}(T+2)^{\frac{3}{2}}}, \quad (13a)$$

$$T = \beta N_o t. \quad (13b)$$

By considering the initial particle number density distribution as Gaussian-like distribution (Eq. (12)), the number density of particles at different times is solved analytically (Eq. (13a)) assuming a constant rate kernel β in Eq. (2). To compare with the numerical model, initial average radius of particles is assumed to be 100 nm, and constant rate kernel as $8k_B T/3\eta$, where k_B is the Boltzmann constant, T is the absolute temperature, and η is the viscosity of particle medium. The ensuing particle size distribution at temperature

300 K and viscosity 0.001cp is compared between the model and analytical solutions at volume fractions of 0.1% (Figure 2(a)) and 0.01% (Figure 2(b)). As shown in Figures 2(a) and 2(b), the number density distribution of particles for different size intervals and at different times is nearly identical for both methodologies, thus validating the present numerical model.

III. EXPERIMENTAL SETUP AND PROCEDURE

Alpha alumina nanoparticles from Inframat Advanced Materials LLC, USA were used in the current experiments. The alumina nanoparticles are specified to be spherical in shape but polydispersed in terms of their sizes with the average particle diameter of about 150 nm. As these alumina nanoparticles are not functionalized, there are no repulsive forces between the alumina nanoparticles in the powder form, with the potential for forming bigger clusters of nanoparticles. Significant energy was required to disperse the nanoparticle clusters apart in de-ionized water, e.g., about 5–16 h of continuous ultrasonication was required to break most of the particles apart. Hydrochloric acid was used to lower the pH from the isoelectric point (pH=9) to induce positive charge on the nanoparticles. Additionally, sodium chloride, electrolyte of the order of milli-moles per liter of nanofluid, was added to create electrostatic double layer around particles as mentioned earlier. Various nanofluids were prepared for the study here, viz., volume fractions of 0.05% and 0.01%, pH values of 3, 3.3, and 4, and electrolyte concentrations at 10^{-3} M and 10^{-4} M. Independent of this, SiC-water nanofluid samples from Argonne National Laboratory were also studied as part of this work.

After ultrasonication a sample was taken and analyzed immediately using a DLS device, NICOMP 380 submicron particle sizer, to obtain the initial PSD as well as at other times. Other light scattering methods to analyze the PSDs are Rayleigh scattering, Rayleigh-Gans-Debye scattering, and Mie scattering. DLS technique used here, also known as quasi-elastic light scattering (QELS) or photon correlation spectroscopy (PCS), measures the intensity of the light scattered by the particles incident by the light waves from source. The DLS device has to be calibrated every day it is used, by analyzing PSD of standard dispersions such as polystyrene latex beads. The NICOMP data for each measurement included the average particle size and standard deviation for both the volume weighted and the number weighted PSDs. According to the NICOMP submicron particle sizer instrument manufacturer, a 5% inaccuracy in the average particle sizes is acceptable. The variations of nanofluid PSDs due to agglomeration with time were studied by analyzing the samples from various nanofluids at different time intervals, viz., 1 day, 2 days, 5 days, and 3 weeks, from the initial fluid preparation.

The initial PSDs of all nanofluids were provided as inputs to the numerical model to solve the coupled population balance equations and obtain distributions of particle sizes in nanofluids after different elapsed times. Measured and calculated nanofluid PSDs were compared and are discussed below.

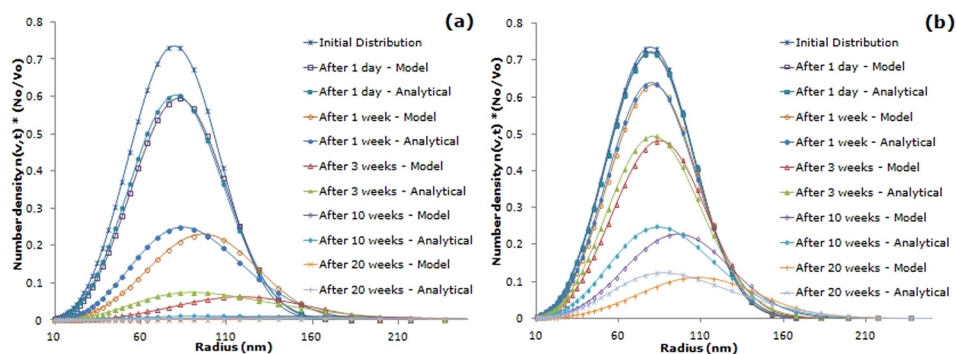


FIG. 2. Number density distributions of particles of different sizes and at different times for initial Gaussian-like distribution at (a) 0.1% and (b) 0.01% volume fractions.

IV. RESULTS AND DISCUSSIONS

Immediately after ultrasonication, $t = 0$ s, each nanofluid was analyzed for the initial particle size distribution, as shown in Figure 3. NICOMP system generates the Gaussian distributions that are relative to the peak value and on a logarithmic scale, and for a better appreciation of the particle size distribution data are presented in Figure 4 using linear abscissa for the measured average particle sizes. The nanofluids have initial average particle sizes around 150 nm as specified by the particle manufacturer. The observed PSDs

of nanofluids obtained using NICOMP-DLS at different times are presented in Figures 5 and 6. All the nanofluid PSDs presented seems to get broader indicating increased agglomeration with time. Both experimental observation and the prediction show that the particle size changes only slightly in 3 weeks for pH of 3, as shown in Figure 5(a). In fact, the experiments indicate that the particle size is smaller after 3 weeks than those after 2 days and 5 days. However, the model predicts a very small level of agglomeration in this nanofluid at this condition. The deviation between the

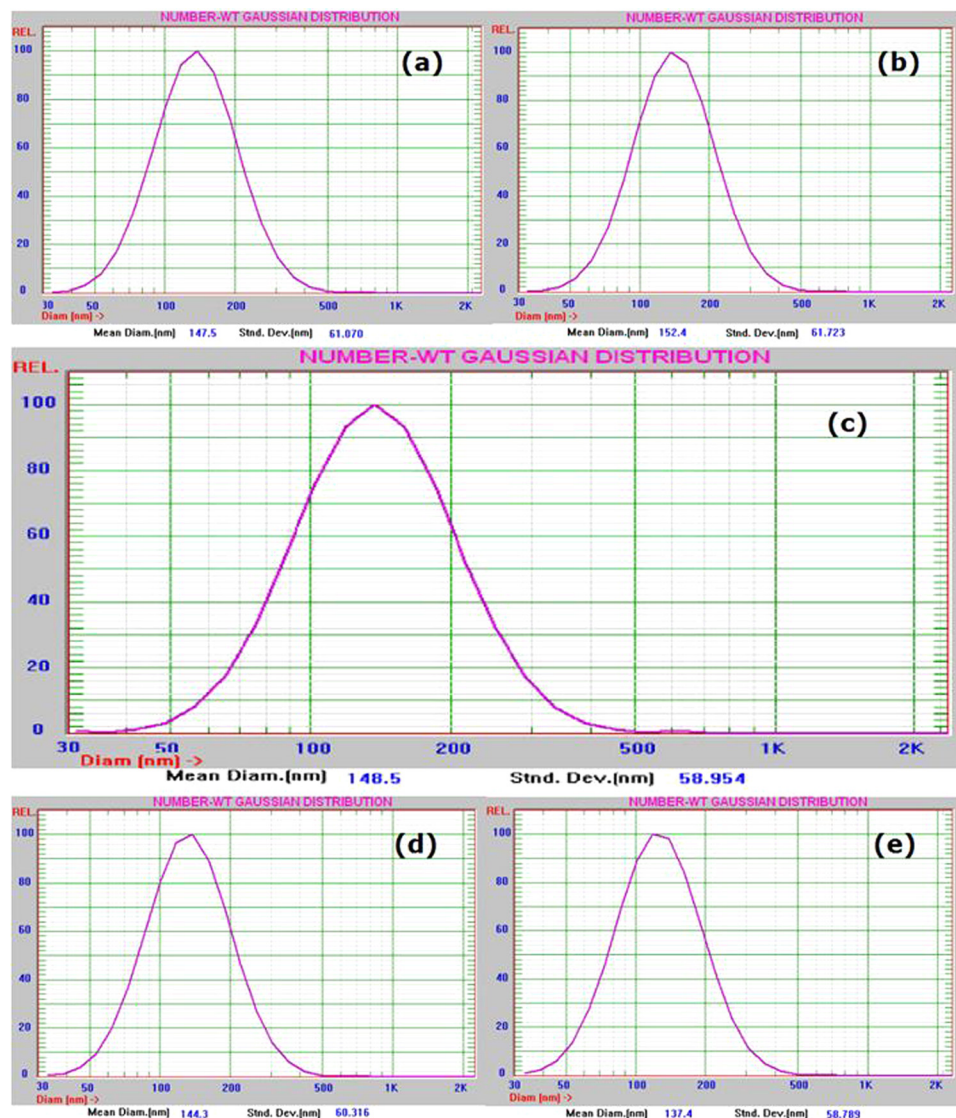


FIG. 3. Number weighted particle size distributions for different alumina-water nanofluids at $t = 0$ s, by NICOMP 380. At volume fraction 0.05%, (a) pH = 3, $C = 10^{-4}$ M, (b) pH = 3.3, $C = 10^{-3}$ M, (c) pH = 4, $C = 10^{-3}$ M, and (d) pH = 4, $C = 10^{-4}$ M. At volume fraction 0.01%, (e) pH = 4, $C = 10^{-4}$ M. C is the concentration of NaCl measured in molarity.

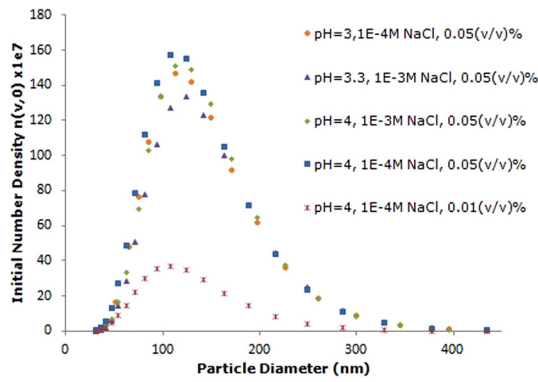


FIG. 4. Initial particle number density distributions for alumina nanofluids, $t = 0$ s.

model and the experimental observation is believed to be the accuracy of the particle measuring device. As mentioned earlier, the NICOMP submicron particle sizer instrument manufacturer has an accuracy of 5% in the average particle size measurement and the particle size variations here are within that experimental uncertainty level. It is believed by the authors that this reverse trend observed in the experiment may not be a new physics that is not covered in the model of this paper. On the contrary, agglomeration level is much higher for pH value of 4 and the measured and predicted particle size in 2 weeks matches, as shown in Figure 5(b).

In a nanofluid, the extent of agglomeration is dependent on the rate of Brownian motion along with the total interparticle interaction energy. Since the Van der Waals attraction energy between the particles cannot be altered easily, to improve stability/shelf life of a nanofluid the electrostatic repulsion energy between the particles needs to be controlled

by varying the pH and electrolyte concentration or other particle functionalization.

With decrease in the pH from 4 to 3, the number of H^+ ions is increased by an order of magnitude. These potential determining ions affect the surface of alumina nanoparticles resulting in a net charge on the surface. These charged particles are surrounded by the counter-ions, in this case Na^+ and Cl^- , forming a Debye layer of ions around the nanoparticles. With increase in the concentration of the counter-ions by increasing the electrolyte concentration, the thickness of the Debye layer can be manipulated.

During the agglomeration process, the smaller particles are prone to have more number of collisions due to their larger diffusion coefficient, and are more likely to form clusters of bigger particles. This can be observed in Figures 5 and 6; the number of smaller particles is decreasing as the number of bigger particles is increasing. Large decrease in the numbers of smaller particles is necessary for a small increase in the number of bigger particles. The total volume of all the nanoparticles per unit volume of nanofluid is a conserved parameter during the agglomeration process.

The independent parameters considered here for the nanoparticle agglomeration model are volume fraction, pH , electrolyte concentration, zeta potential, Hamaker constant, and temperature. The PSDs generated using the numerical model are compared with experimental measurements in Figures 5 and 6. The model predictions start with the initial average particle sizes and standard deviations of both the particle number and volume weighted distributions along with the independent variables considered. The agreement between the experimental data and numerical model predictions is good and the differences can be attributed to the assumptions made for the theoretical derivations of the

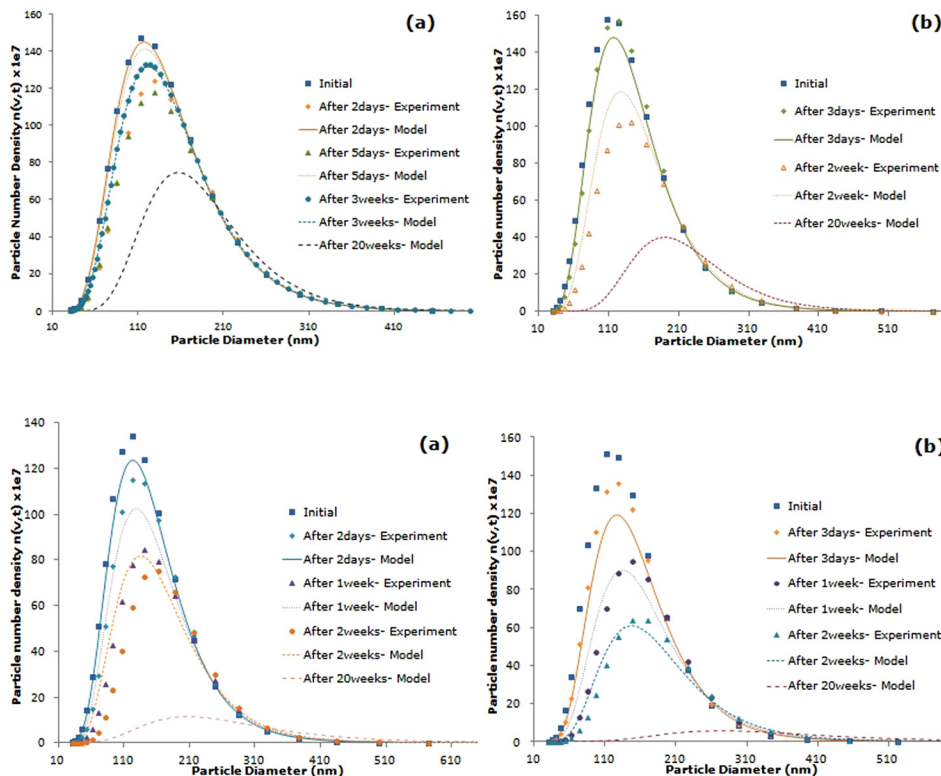


FIG. 5. Particle number density distributions at different times for alumina nanofluid at 0.05% (v/v) with 10^{-4} M of NaCl, (a) pH = 3 and (b) pH = 4.

FIG. 6. Particle number density distributions at different times for alumina nanofluid at 0.05% (v/v) with 10^{-3} M of NaCl, (a) pH = 3.3 and pH = 4.

TABLE I. Parameters of alumina nanofluids with 0.05% (v/v) at different pH and electrolyte concentration.

Alumina nanofluid	Total ionic concentration (M)	Zeta potential (mV)	Debye length (nm)
$pH = 3, 10^{-4}$ M NaCl	1.2×10^{-3}	62.1	12.6
$pH = 3.3, 10^{-3}$ M NaCl	2.5×10^{-3}	61.9	8.71
$pH = 4, 10^{-3}$ M NaCl	2.1×10^{-3}	40	9.50
$pH = 4, 10^{-4}$ M NaCl	3.0×10^{-3}	43.4	25.1

expressions for inter-particle potential energies, uncertainties in the measurement of zeta potential and experimental procedures in general.

Nanofluids with $pH = 4$ and 10^{-3} M NaCl corresponding to lower zeta potential and smaller Debye length were observed to agglomerate at faster rates compared to others, as shown in Table I.

Alumina nanofluid with a pH of 3 and 10^{-4} M NaCl is observed to have very slow rate of agglomeration compared to others and that is attributed to higher zeta potential and larger Debye length for these conditions. With increase in the counter-ion concentration by increasing electrolyte concentration, the thickness of the electrical double layer decreased (see Table I) thus decreasing the repulsive forces and total potential energies between particles (Figure 7). Among the alumina nanofluids experimented with here, the nanofluid with lower pH and lower electrolyte concentration (with $pH = 3$ and 10^{-4} M NaCl) had smaller average particle sizes compared to those with higher pH and higher electrolyte concentration (with $pH = 3.3$ and 10^{-3} M NaCl). This indicates longer shelf life for alumina nanofluid with $pH = 3$ and 10^{-4} M NaCl compared to alumina nanofluid with

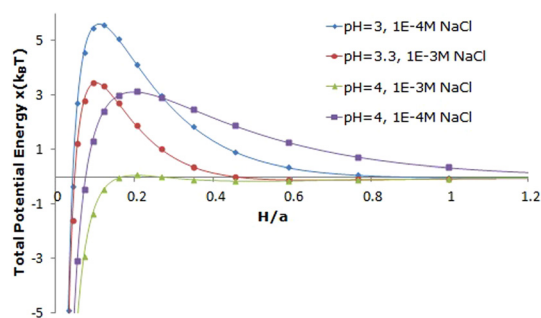


FIG. 7. The total interaction energy between two alumina particles of diameter 150 nm in water. " H " is the distance between the surfaces of particles of radius " a ."

$pH = 4$ and 10^{-3} M NaCl; and this process should be considered with potential pH changes with time due to oxidation and/or other chemical changes.

The average particle diameters from PSDs for alumina nanofluids with different properties and at different times can be used to quantitatively estimate the extent of agglomeration. Since the results of the numerical model compare quite favorably with experimental results, the model presented here can be used to determine the anticipated average particle diameter of alumina nanofluids for any shelf time. As indicated in Table II, the average particle size of alumina nanofluid-3 ($pH = 4$ and 10^{-3} M in Table II) with lower zeta potential (see Table I) increased by 28% in 2 weeks. On the other hand, alumina nanofluid-1 ($pH = 3$ and 10^{-4} M in Table II) with a higher zeta potential (see Table I) increased by only 5% in 2 weeks. This brings out the dependence of agglomeration on zeta potential among others; alumina nanofluid-3 compared to alumina nanofluid-2. The average

TABLE II. Average particle diameter (nm) and standard deviation (nm) for particle size distributions from experimental analysis and numerical modeling at different times for alumina nanofluids. C is the concentration of electrolyte in Molarity.

Alumina nanofluid	Properties	Time	Mean particle diameter (nm), standard deviation (nm)	
			Experiment	Model
1	0.05% (v/v), $pH = 3$, $C = 10^{-4}$ M	0 s	148, 61	148, 61
		2 days	158, 61	148, 61
		5 days	158, 63	150, 61
		3 weeks	153, 62	156, 62
		20 weeks	187, 65	
2	0.05% (v/v), $pH = 3.3$, $C = 10^{-3}$ M	0 s	152, 62	152, 62
		2 days	161, 62	155, 63
		1 week	175, 67	163, 67
		2 weeks	186, 64	172, 71
		20 weeks	274, 124	
3	0.05% (v/v), $pH = 4$, $C = 10^{-3}$ M	0 s	149, 59	149, 59
		3 days	154, 60	158, 63
		1 week	175, 62	169, 68
		2 weeks	190, 69	185, 76
		20 weeks	341, 137	
4	0.05% (v/v), $pH = 4$, $C = 10^{-4}$ M	0 s	144, 60	144, 60
		3 days	147, 59	148, 61
		2 weeks	165, 64	158, 63
		20 weeks	222, 74	

particle size of alumina nanofluid-4 ($pH = 4$ and 10^{-4} M in Table II) increased by 14% in 2 weeks as compared to alumina nanofluid-3 with 28% increase in 2 weeks. This is attributed to the bigger Debye length for alumina nanofluid-4 as compared to nanofluid-3 (see Table I). It appears the agglomeration is strongly dependent on pH, ionic concentration, and the related zeta potential. In order to estimate the shelf life of these nanofluids, numerical model is used to predict average particle size in nanofluids after 20 weeks. The numerical model predicted that in 20 weeks the average particle size in alumina nanofluid-3 will increase by 128%, whereas the average particle size in alumina nanofluid-1 will increase by only 25%. Such increases in average particle sizes in a nanofluid due to agglomeration are not desirable for the application of nanofluids in industrial applications. In the above example, alumina nanofluid-3 with faster agglomeration compared to alumina nanofluid-1 has shorter than 20 weeks of shelf life, which could be significant for many industrial applications.

V. SUMMARY

Nanofluids have been used in many industrial applications and have been touted to be very useful as heat transfer fluid with anticipated enhancement. Quite often the nanoparticles used are specified to be of particle sizes distributions that they were in the powder condition. As indicated in the present work, there could be significant agglomeration of particles in nanofluids as a function of time (2 to 4 weeks) and other independent parameters considered here to characterize the alumina nanofluids considered here. A numerical model to predict the agglomeration of particles in a nanofluid is presented and the results of the model have been verified with alumina nanofluids and their particle size distribution measurements as a function of time. The numerical model uses minimal empiricism and is based on first principles and describes agglomeration based on independent parameters such as particle volume fractions, pH , electrolyte ionic concentrations, and zeta potential of the nanofluid. Agglomeration of particles in nanofluids appears to be strongly dependent on pH , electrolytic ionic concentration, and the related zeta potential of the nanofluid. Such models and the predictive capabilities can be quite useful to evaluate the shelf life and useful life of nanofluids in industrial applications.

- ¹Y. K. Park, E. H. Tadd, M. Zubris, and R. Tannenbaum, "Size-controlled synthesis of alumina nanoparticles from aluminum alkoxides," *Mater. Res. Bull.* **40**, 1506–1512 (2005).
- ²J. Eastman, S. Choi, S. Li, W. Yu, and L. Thompson, "Anomalous increased effective thermal conductivities of ethylene glycol-based nanofluids containing copper nanoparticles," *Appl. Phys. Lett.* **78**, 718–720 (2001).
- ³S. Lee, S. Choi, S. Li, and J. Eastman, "Measuring thermal conductivity of fluids containing oxide nanoparticles," *J. Heat Transfer* **121**, 280–289 (1999).
- ⁴F. London, "The general theory of molecular forces," *Trans. Faraday Soc.* **33**, 8b-12 (1937).
- ⁵A. Islam, B. Chowdhry, and M. Snowden, "Heteroaggregation in colloidal dispersions," *Adv. Colloid Interface Sci.* **62**, 109–136 (1995).
- ⁶S. K. Das, N. Putra, and W. Roetzel, "Pool boiling characteristics of nanofluids," *Int. J. Heat Mass Transfer* **46**, 851–862 (2003).
- ⁷C.-H. Lo and T.-T. Tsung, "Low-temperature effect on the stability of CuO nanofluid," *Rev. Adv. Mater. Sci.* **10**, 64–68 (2005).
- ⁸D. Lee, J.-W. Kim, and B. G. Kim, "A new parameter to control heat transport in nanofluids: Surface charge state of the particle in suspension," *J. Phys. Chem. B* **110**, 4323–4328 (2006).
- ⁹E. V. Timofeeva, A. N. Gavrilov, J. M. McCloskey, and Y. V. Tolmachev, "Thermal conductivity and particle agglomeration in alumina nanofluids: Experiment and theory," *Phys. Rev. E* **76**, 061703/1–061703/16 (2007).
- ¹⁰J.-H. Lee, K. S. Hwang, S. P. Jang, B. H. Lee, J. H. Kim, S. U. Choi, and C. J. Choi, "Effective viscosities and thermal conductivities of aqueous nanofluids containing low volume concentrations of Al₂O₃ nanoparticles," *Int. J. Heat Mass Transfer* **51**, 2651–2656 (2008).
- ¹¹Y. Yang, A. Oztekin, S. Neti, and S. Mohapatra, "Particle agglomeration and properties of nanofluids," *J. Nanopart. Res.* **14**, 852/1–852/10 (2012).
- ¹²S. Kumar and D. Ramkrishna, "On the solution of population balance equations by discretization—II. A moving pivot technique," *Chem. Eng. Sci.* **51**, 1333–1342 (1996).
- ¹³N. Rao, "Simulations for modelling of population balance equations of particulate processes using discrete particle model," Ph.D. thesis (Otto-von-Guericke University, Magdeburg, Germany, 2009).
- ¹⁴M. Smoluchowski, "Mathematical theory of the kinetics of the coagulation of colloidal solutions," *Z. Phys. Chem.* **92**, 129–168 (1917).
- ¹⁵R. J. Hunter and L. R. White, *Foundations of Colloid Science* (Clarendon Press, Oxford, 1987).
- ¹⁶B. V. Derjaguin and L. Landau, "Theory of the stability of strongly charged lyophobic sols and of the adhesion of strongly charged particles in solutions of electrolytes," *Acta Physicochim* **14**, 633–662 (1941).
- ¹⁷E. J. W. Verwey and J. T. G. Overbeek, *Theory of the Stability of Lyophobic Colloids* (Elsevier, Amsterdam, 1948).
- ¹⁸H. C. Hamaker, "The London–van der Waals attractions between spherical particles," *Physica IV* **4**, 1058–1072 (1937).
- ¹⁹P. Debye and E. Hückel, "The theory of electrolytes. I. Lowering of freezing point and related phenomena," *Zeitschr. Physik* **24**, 185–206 (1923).
- ²⁰J. E. Sader, S. L. Carnie, and D. Y. Chan, "Accurate analytic formulas for the double-layer interaction between spheres," *J. Colloid Interface Sci.* **171**, 46–54 (1995).
- ²¹R. Hogg, T. W. Healy, and D. W. Fuerstaneau, "Mutual coagulation of colloidal dispersions," *Trans. Faraday Soc.* **62**, 1638–1651 (1966).
- ²²W. T. Scott, "Analytic studies of cloud droplet coalescence I," *J. Atmos. Sci.* **25**, 54–65 (1968).